



HAL
open science

Thermodynamic properties assessment of working mixtures water + alkylphosphonate based ionic liquids as innovative alternatives working pairs for absorption heat transformers

El-Shaimaa Abumandour, Fabrice Mutelet, Dominique Alonso

► **To cite this version:**

El-Shaimaa Abumandour, Fabrice Mutelet, Dominique Alonso. Thermodynamic properties assessment of working mixtures water + alkylphosphonate based ionic liquids as innovative alternatives working pairs for absorption heat transformers. Applied Thermal Engineering, 2020, 181, pp.115943 -. 10.1016/j.applthermaleng.2020.115943 . hal-03492442

HAL Id: hal-03492442

<https://hal.science/hal-03492442>

Submitted on 9 Sep 2022

HAL is a multi-disciplinary open access archive for the deposit and dissemination of scientific research documents, whether they are published or not. The documents may come from teaching and research institutions in France or abroad, or from public or private research centers.

L'archive ouverte pluridisciplinaire **HAL**, est destinée au dépôt et à la diffusion de documents scientifiques de niveau recherche, publiés ou non, émanant des établissements d'enseignement et de recherche français ou étrangers, des laboratoires publics ou privés.



Distributed under a Creative Commons Attribution - NonCommercial 4.0 International License

Thermodynamic properties assessment of working mixtures {water + alkylphosphonate based ionic liquids} as innovative alternatives working pairs for absorption heat transformers.

El-Shaimaa Abumandour, Fabrice Mutelet *, Dominique Alonso

Laboratoire Réactions et Génie des Procédés (CNRS UMR 7274), Université de Lorraine, 1 rue Grandville, 54000 Nancy, France.

Abstract. Based on a continuously developing portfolio of ionic liquids, the aim of this work is to evaluate the performance of new working pairs composed of {water + alkylphosphonate based IL} as alternative working pairs for absorption heat transformers. Therefore, thorough thermodynamic measurements were conducted for three alkyl phosphonate based ionic liquids and their aqueous binary systems. Experimental measurements of vapor-liquid equilibrium, heat capacity, density and excess enthalpy were measured and successfully represented using NRTL model and adequate equations. Thermal performances of single stage absorption heat transformer were numerically simulated. The influence of the temperature sources and sinks was studied. The best coefficient of performance was obtained with mixtures of water and 1-ethyl-3-methylimidazolium methylphosphonate. The typical coefficient of performance values for this mixture is found to be between 0.40 and 0.45 depending on the temperature conditions. This value is 10% lower than that observed with the classically used {water + lithium bromide} mixture. Nevertheless, {water + ionic liquid} mixture has a wider operating temperature range than conventional working pairs. The higher circulation ratio observed with the proposed mixtures may increase pumping cost.

Keywords: Ionic liquids, Thermodynamic properties, absorption heat transformers, Coefficient of performance.

(*) author to whom the correspondence should be addressed: e-mail: fabrice.mutelet@univ-lorraine.fr - Telephone number: +33 3 83 17 51 31 - Fax number: +33 3 83 17 53 95

Nomenclature

AHT	Absorption heat transformers (-)
ARD	Average relative deviation (-)
COP	Coefficient of performance (-)
E181	Tetraethylene glycol dimethyl ether (-)
f	Circulation ratio (-)
HFCs	Hydroflorocarbons (-)
IL	Ionic liquids (-)
NMR	Nuclear Magnetic Resonance (-)
NRTL	Nonrandom two-liquid model (-)
OF	Objective function (-)
SSAHT	Single stage absorption heat transformers (-)
TFE	2, 2, 2-trifluoroethanol (-)
α_{ij}	temperature dependent equations parameter for Δg_{ij} (J.mol ⁻¹)
b_{ij}	temperature dependent equations parameter for Δg_{ij} (J.mol ⁻¹ .K ⁻¹)
A_i and B_i	Parameters of Redlich-Kister equation (-)
a_i and b_i	temperature dependent equations parameter for A_i or B_i

C_p	Mass heat capacity ($\text{kJ.kg}^{-1}.\text{K}^{-1}$)
C_p^E	Mass excess heat capacity ($\text{kJ.kg}^{-1}.\text{K}^{-1}$)
$C_{p,i}$	Mass heat capacity of the pure compound i ($\text{kJ.kg}^{-1}.\text{K}^{-1}$)
g_{ij}	Energy of interaction between species i and j (J.mol^{-1})
h_i	Enthalpy of stream ($i = 1, 2, \dots, 10$) (kJ.kg^{-1})
H^E	Mass excess enthalpy (kJ.kg^{-1})
m	Mass of the sample (kg)
\dot{m}_i	Mass flow rate of stream ($i = 1, 2, \dots, 10$) (kg.s^{-1})
p	pressure (kPa)
Q	Heat load (kJ.s^{-1})
Q_s, Q_b	Heats measured for the blank and for the sample for the increment temperature ΔT
q	available heat output (Watt)
T_H, T_M, T_L	High, medium and low temperature level (K, °C)
T	Temperature (K)
Δt	Gross temperature lift (K, °C)
ΔT	Increment of temperature (K, °C)
VLE	Vapor liquid equilibrium (T (K), P (kPa))

V^E	Excess molar volume ($\text{cm}^3 \cdot \text{mol}^{-1}$)
x_i^m	Mass fraction of species i where $i = 1,2$ (-)
x	Mole fraction (-)
x^m	Mass fraction (-)
Δx^m	Difference of mass fraction between strong and weak solutions (-)

Subscripts

A	Absorber (-)
C	Condenser (-)
E	Evaporator (-)
G	Generator (-)
ss	Strong solution (-)
w	Water (-)
ws	Weak solution (-)
sol	Solution (-)

Exponent

s	Saturation
---	------------

E Excess

Greek letters

α Non-random parameter of NRTL model (-)

τ Interaction parameter of NRTL model (-)

ρ Density (g.cm⁻³)

γ_i Activity coefficient of species i , $i = 1, 2$, (1 = refrigerant, 2 = absorbent) (-)

Δg_{ij} Interaction parameter of NRTL model (J.mol⁻¹)

Ionic liquids

[BMIM] 1-butyl-3-methylimidazolium (-)

[DEMA] diethylmethylammonium (-)

[DMIM] 1,3-dimethylimidazolium (-)

[EMIM] 1-ethyl-3-methylimidazolium (-)

[HMIM] 1-hexyl-3-methylimidazolium (-)

[HOEtMIM] 1-(2-hydroxyethyl)-3-methylimidazolium (-)

[MIM] methylimidazolium (-)

[P₆₆₆₁₄] trihexyl(tetradecyl)phosphonium (-)

[Ac] acetate (-)

[BF₄] tetrafluoroborate (-)

[Br] bromide (-)

[DCA] dicyanamide (-)

[DMP] 1,3-dimethylimidazolium dimethylphosphate (-)

[EPH] ethylphosphonate (-)

[EtSO₄] ethylsulfate (-)

[MeSO₃] methanesulfonate (-)

[MeSO₄] methyl sulfate (-)

[MPh] methylphosphonate (-)

[OMs] methane sulfonate (-)

[OTf] or [Triflate] trifluoromethanesulfonate (-)

[PF₆] hexafluorophosphate (-)

[SCN] thiocyanate (-)

[TCM] tricyanomethanide (-)

[TFA] trifluoroacetate (-)

[Tf₂N] bis(trifluoromethylsulfonyl)imide (-)

[TFES] 1,1,2,2-tetrafluoroethanesulfonate (-)

[TOS] tosylate (-)

1. Introduction

Industrial activities and their byproducts have strong impact on the natural resources, primary energy (non-renewable) sources and raw materials cycle. Positive effects from new technologies may be observed through the enhancement of the economic growth and their answer to the human needs. Meanwhile, they may be negative by adding pollutants, greenhouse gases, CO₂ emissions and non-degradable wastes and/or hazardous materials to the environment and by depleting both natural and energy resources. Accordingly, researchers have to pay attention to the negative environmental impact due to the strong human and industrial activities[1].

In industries, large amounts of low temperature waste heat discharge into waterbodies and/or the atmosphere [2]. One way to increase the efficiency of processes should be to upgrade and reuse this thermal waste heat streams. [3]

Absorption cycles are considered as a suitable solution for a rational use of waste heat and key for reducing CO₂ footprint. One of the most promising devices for energy savings is the absorption heat transformer (AHT). In this field of application, AHT can use waste heat to produce useful thermal energy at higher temperature level for industrial and domestic applications [4]. Nevertheless, the performances of AHT remain low (only 30 to 50% of the driving waste heat is effectively upgraded to an interesting temperature level [5]). The commonly used working fluids in AHT are {water + LiBr} and {ammonia + water}. However, these working fluids have technical drawbacks such as corrosion and crystallization, while ammonia is toxic. Those technical limitations lead to long payback periods. However, these problems can be avoided if these working pairs are replaced by new alternatives. [6] Essential efforts to propose new working fluids or multistage structures have still not allowed to widespread this technology.[7]

It is now well established that ionic liquids (ILs) may be used in various industrial applications [8]. These solvents consist of an asymmetric, bulky organic cation and a weakly coordinating organic or inorganic anion. The large number of combinations anion/cation/cation substituents enhance the ability to 'fine tune' the solvent properties for a specific purpose. The most interesting properties of ILs are their negligible vapor

pressure, non-flammability, nontoxicity, good thermal stability, low melting points. Moreover, ILs are liquid in a large range of temperature (from 25 to 200°C).

The use of ILs in chemical engineering covers a large domain of applications. Among others, they showed interesting performances in separation processes (biomass conversion, desulfurization...) but also in the field of energy (absorption heat transformer, storage, battery, solar cells).

The use of binary mixtures {H₂O + IL} or {ethanol + IL} in AHT may enhance absorption of large amount of refrigerant under low temperature conditions and hence, yield to high coefficient of performance (COP) [9,10]. In the last decade, researchers have been proposing numerous ILs with water mixtures and other solvents, although much effort has been done on the subject, yet more is required [11].

Thermodynamic and transport properties of binary systems are required to design any process involving ionic liquids on an industrial scale. In the case of AHT, vapor- liquid equilibrium, heat capacity, excess enthalpy and density are necessary for simulations and COP evaluations. Vataschin and Dohnal contribute to the knowledge of thermodynamic properties of [EMIM] based ILs containing [MeSO₃], [MeSO₄], [DMP],[12], [Br], [Tos], [13][SCN], [DCA] [14], [TCM] [15] and [TFES] and [OTf] [16]. Most systems containing {H₂O+ [EMIM] based IL} exhibit an S-shaped excess heat capacity. Excess enthalpy values are negative with the anions [MeSO₃], [MeSO₄], [DMP], [Br], [Tos], [SCN], positive with [TCM] and sharply with [SCN] and [DCA] anions.

The performance of {H₂O + IL} as working fluids was essentially estimated for the absorption refrigeration cycle [6]. In this comparative study, performance of absorption heat transformer was evaluated based on thermodynamic data of 11 different ionic liquids gathered from literature. Simulation results showed that for the investigated working pairs {H₂O + IL}; COP is close, yet lower than {H₂O + LiBr}. However, this tiny disadvantage can be balanced by the ability of these working pairs to increase gross

temperature lifts (Δt) and the possibility of prohibiting corrosion and decreasing and/or avoiding crystallization. Under the same operation conditions, COP values for the studied binary systems showed the hereunder behavior:

[DMIM][DMP] > [HOEtMIM][Cl] > [EMIM][Ac] > [DEMA][OMs] > [EMIM][TFA] > [EMIM][DMP] > [BMIM][BF₄] > [EMIM][OTf] > [EMIM][EtSO₄] > [BMIM][OTf].

Zheng et al. [10] have presented the state of the art on the knowledge of thermodynamic properties of binary systems containing an IL and an hydrocarbon, an hydrofluorocarbon, ammonia, water or an alcohol. The coefficient of performance obtained using {H₂O + IL} ranges from 0.52 to 0.83. This study shows that the efficiency obtained are lower than the COP value obtained with {H₂O + LiBr}. The best results are observed with {H₂O+[DMIM][DMP]} and {H₂O+ [DMIM][Cl]}. Simulation of {HFC + IL} binary systems leads to the conclusion that the COP values are particularly low while they range from 0.12 to 0.39. Similar conclusion is obtained with {NH₃ + IL}. Wang and Ferreira [17] evaluated the possible use of {NH₃ + IL} working pairs in AHT. As expected, the circulation ratios obtained with {NH₃ + IL} is between 6 to 24 times higher than the value obtained with {NH₃ + H₂O}. The authors conclude that {NH₃ + [MIM][DMP] or [EMIM][Tf₂N] or [EMIM][SCN] or [BMIM][BF₄]} mixtures present higher COP values than {NH₃ + H₂O}. Sun et al have studied three new R1234yf/IL working pairs for the refrigeration. [18] This work shows that phosphonium based ILs are more efficient than dialkylammonium based ILs. The highest COP value for R1234yf/[P₆₆₆₁₄][Cl] was found to be 0.43. Song et al. proposed a new power/cooling system composed of an absorption-compression refrigeration cycle and an organic Rankine cycle. [19] Working fluids containing R1234ze (E) and dialkylimidazolium tetrafluoroborate were evaluated in the refrigeration cycle. In this study, it appears that the COP values are related to the alkyl

chain length. Liu et al. propose to enhance the efficiency of the absorption refrigeration cycle by using working fluids containing R1234yf and [HMIM][OTf], [HMIM][BF₄] or [HMIM][PF₆]. [20] The use of { R1234yf + [HMIM][OTf] } as working fluid in absorption-compression hybrid refrigeration systems allows to obtain a COP value at least 1.5 higher than those in classical absorption refrigeration system. Chen *et al.* [21] found that both COP and efficiency for heat recovery η_{ex} for {H₂O + [DMIM][DMP]} and {CH₃OH + [DMIM][DMP]} as working fluids are lower than the conventional system {H₂O + LiBr} by 10%. Nevertheless, the gross temperature left for both systems is higher than {H₂O + LiBr}.

The performance of a single stage absorption heat transformer cycle using dimethylimidazolium methylsulfate or 1-ethyl-3-methylimidazolium methylsulfate with water was assessed based on the measured thermodynamic data and on the mass and energy balance for each component of the system. [9] Simulation results indicate that the COP of (methylsulfate based IL + water) is slightly lower than {H₂O + LiBr}. However, the cycle using {H₂O + ILs} systems allow to extend the operating temperature range and to relieve the disadvantages of crystallization and corrosion caused by {H₂O + LiBr}.

In 2011, Murshed et al [22] proposed to use Ionanofluids, a suspension of nanoparticles in ionic liquids for heat transfert applications. Their first study using [BMIM][Tf₂N] and [BMIM][EtSO₄] show that the presence of multi-walled nanotubes in this IL enhance their thermal conductivity of about 1.3. The recent review of Minea and Murshed [23] indicates that the new class of fluids possess interesting thermal properties but their physico-chemical properties are not well-known and some disagreements are found in the literature. It is also found in the literature that phosphonium based ILs are not good

candidate to produce stable suspension with Multiwalled carbon nano tubes [24]. More recently, numerous papers proposed to add IL in traditional working fluids. Luo et al. [25] investigated the mixture $\{\text{LiNO}_3 + [\text{DMIM}][\text{DMP}] + \text{H}_2\text{O}\}$ as a potential working pair. The COP value of $\{\text{LiNO}_3 + [\text{DMIM}][\text{DMP}] + \text{H}_2\text{O}\}$ is very close to those obtained with $\{\text{LiNO}_3 + \text{H}_2\text{O}\}$ or $\{\text{LiBr}/\text{H}_2\text{O}\}$. Yang et al. [26] studied the thermodynamic properties of the mixture $\{\text{LiBr} + [\text{EMIM}][\text{Cl}] + \text{H}_2\text{O}\}$. Their work showed that adding $[\text{EMIM}][\text{Cl}]$ may reduce the crystallization temperature up to 30°C of $\{\text{LiBr} + \text{H}_2\text{O}\}$ and increase the absorption capacity.

Dialkylimidazolium alkylphosphonate were found to be suitable for the extraction of cellulose from biomass [27] or diesel desulfurization [28]. The main advantage to use this family of IL is their low costs (400-500€/kg), their decomposition temperature (higher than 250°C), their moderate viscosity [29]. Moreover, it was found that a passivation layer is formed at the surface of S235 carbon steel specimens in presence of $[\text{EMIM}][\text{MPh}]$ [30].

The main objective of this study is to evaluate the performance of (alkylphosphonate based ILs + water) as working fluids in AHT and more precisely: $\{\text{H}_2\text{O} + \text{ILs (1,3-dimethylimidazolium methylphosphonate } [\text{DMIM}][\text{MPh}] \text{ or 1-ethyl-3-methylimidazolium methyl phosphonate } [\text{EMIM}][\text{MPh}] \text{ or 1-ethyl-3-methylimidazolium ethyl phosphonate } [\text{EMIM}][\text{EPh}])\}$. To do so, thermodynamic properties (vapor liquid equilibria, heat capacity, density and excess enthalpy) of the pure ionic liquids and their binary mixtures with water were determined in a large range of temperature.

2. Experimental section

2.1. Materials

The ILs studied were purchased commercially from Solvionic. Chemicals used as reference fluids and for validation of the measurements as n-hexane (purity > 99 %), n-heptane (purity > 99 %), Tetrachloroethylene (purity > 99 %), n-undecane (purity > 99%) and n-dodecane (purity > 99 %) were purchased from Sigma Aldrich and Acros Organics, respectively. Ultrapure water was provided by Purelab Ultra system (> 18 M Ω ·cm) (ELGA LabWater). Mercury with a purity of 99.99 % was purchased from Sigma Aldrich.

Table 1 shows chemical structure, CAS number, abbreviation, provenance and purity (provided by supplier) of ILs. Water content was determined with a TIM550 Karl Fischer volumetric titration (Titralab) using the HYDRANAL-Solvent E as analyte (provided by Sigma-Aldrich). The water content determined by the Karl Fischer coulometric titrator (Mettler Toledo) are also given in Table 1. In addition, the structure of ILs was checked with ¹H NMR (300 MHz, (CH₃)₂CO, ppm) prior to experimentation. ¹H NMR spectra are given in supporting information (Figures S1-S3).

2.2. Sample preparation

To remove traces of water and volatile compounds, each ionic liquid was dried at moderate temperature (323.15 K) under high vacuum during 24 h before sample preparation. All binary mixtures (H₂O + alkylphosphonate based IL) were prepared by weighing a precise amount of IL and ultrapure water using a microbalance (Sartorius) with an uncertainty of $\pm 10^{-4}$ g. Homogeneity was ensured by using Teflon coated magnet stirrer for 30 min. All samples were prepared immediately prior to the measurements to avoid any variation in composition.

2.3. Thermodynamic measurements

2.3.1. Vapor liquid equilibrium (VLE)

VLE measurements were carried out using the experimental device presented in Figure 1. The procedure used in this work were fully described in our previous works [9]. Briefly, the apparatus mainly consists of an equilibrium cell (250 cm³) maintained at fixed temperature using a Fisher Scientific Polystat 5D+37 oil bath. The cell is connected to a condenser in order to avoid any loss of water vapor. The temperature of the condenser cooled with glycol solution is fixed at 263.15 K. The temperature inside the equilibrium cell is measured using a temperature sensor thermocouple (T900 series) calibrated with high measuring accuracy (T900 ± 0.03 °C). The system pressure is measured using a pressure transducer (Druck-PMP4010) with the accuracy of (± 0.04 % FS BSL).

The measurement requires a sample volume of about 50 cm³ into the cell. During the experiment, the solution is stirred using a stir bar. Firstly, vacuum is established in all the apparatus using the pump and the working pressure is fixed using the valve. Secondly, the mixture is brought to its bubble point by slowly increasing the temperature. When the temperature is stable, the vapor-liquid equilibrium is reached. The experimental apparatus was validated by measuring the bubble points of pure ultrapure water, n-hexane and n-heptane. Comparison of the saturated vapor pressure measured in this work and those published in the literature [31–33] are given in supporting information (Tables S1-S3). Deviation between experimental data and those published in the literature was less than 0.2%. The composition, temperature and pressure ranges are given in Table S4.

2.3.2. Heat capacity (C_p)

The heat capacity of pure ILs and their binary mixtures with water was measured using a differential scanning calorimeter Micro-DSCIII (Setaram, France). A detailed procedure is given in previous works [9]. About 200-400 mg of the sample was introduced into the sample cell. The cell is then hermetically sealed with a lid. The heat capacity measurements were performed within temperatures ranging from 293.15 K to 338.15 K at

a heating rate of 0.15 K.min⁻¹. The determination of heat capacity is based on stepwise method. Two runs are performed while it requires the knowledge of heat flow signals of both empty measuring and reference vessels (blank) and of the measuring vessel containing a mass m_s of the sample. Heat capacity is calculated according to the following equation:

$$C_p = \frac{Q_s - Q_b}{m_s \times \Delta T} \quad (1)$$

Where Q_s and Q_b corresponds to the heats measured for the blank and for the sample for the increment temperature ΔT , respectively. m_s is the mass of the sample in the measuring vessel.

In order to check the reliability of the apparatus, heat capacity of ultra-pure water was measured and compared to literature. Comparison of C_p data of pure water measured in this work and those published in the literature are presented in Table S5. [34] Experimental results are in good agreement with literature within an ARD of 0.18%.

2.3.3. Density (ρ)

The density measurements were performed using Anton Paar DMA 60 digital vibrating-tube densimeter, with a DMA 512P measuring cell [9]. Samples were charged into the vibrating tube carefully using a syringe to avoid gas bubbles occurrence. The measurements for both pure ILs and binary mixtures were performed at temperature range (293.15-323.15 K) at atmospheric pressure. All measurements were repeated three times. The densimeter was calibrated using n-Dodecane, n-Undecane and tetrachloroethylene as reference fluids. The standard uncertainty of density measurements was found to be $u(\rho) = 0.5 \text{ kg m}^{-3}$.

2.3.4. Excess enthalpy (H^E)

Excess enthalpy measurements of binary mixtures ($\text{H}_2\text{O} + \text{IL}$) were obtained using a Setaram C80 calorimeter which is well described in literature [9]. The specific reversal mixing cell has two separate compartments. In the bottom compartment is placed a precise amount of the component having the highest density. A lid is put on this part and

mercury is added to completely isolate the component. Then, the second component was introduced in the mixing cell. The H^E measurements were carried out at 312.92 K at atmospheric pressure. The mixing occurs when the cell is rotated vertically through 180°. The excess enthalpy is obtained by integration of the heat flow peak obtained during the mixing. Each measurement is repeated at least two times. The experimental uncertainty associated with this method is estimated to be $\pm 1\%$ considering the propagation of error and the ability to reproduce measurements with different samples over time.

3. Results and discussion

3.1.1. Vapor liquid equilibrium (VLE)

VLE measured for the 3 binary systems {H₂O + ILs} are listed in the supplementary material Tables S6-S8. No VLE data for the three binary systems studied in this work were found in the literature. Experimental data are shown in supplementary material Figure S4. The {water + alkylphosphonates based ionic liquid} systems have activity coefficients of water smaller than unity over the entire composition range indicating stronger unlike interactions (IL/water) than like interactions (IL/IL and water/water). This behavior was also found for various families of ILs in the literature [35,36]. With respect to the anion, the activity coefficients and vapor pressure values decrease as follows: [EPh]⁻>[MPH]⁻. This means that methylphosphonate anion leads to a greater interaction with water molecules.

The activity coefficient of the solute in the mixture was correlated using the NRTL model [37]:

$$\ln \gamma_1^{\text{NRTL}} = x_2^2 \left[\tau_{21} \left(\frac{G_{21}}{x_1 + x_2 G_{21}} \right)^2 + \frac{\tau_{12} G_{12}}{(x_2 + x_1 G_{12})^2} \right] \quad (2)$$

$$\text{with } G_{ij} = \exp(-\alpha_{ij} \tau_{ij}), \tau_{ij} = \frac{g_{ij} - g_{ji}}{RT} = \frac{\Delta g_{ij}}{RT} \quad (3)$$

The NRTL parameters (g_{12} - g_{22} , g_{21} - g_{11}) are those which minimize the following objective function:

$$OF = \sum_{i=1}^N (\gamma_i^{calc} - \gamma_i^{exp})^2 \quad (4)$$

In order to consider temperature dependency, a linear temperature dependent relation for the interaction parameters Δg_{ij} was used:

$$\Delta g_{ij} = a_{ij} + b_{ij}T \quad (5)$$

The regressed NRTL parameters (a_{12} , a_{21} , b_{12} , b_{21}) are presented in Table 2 for each system. The predicted bubble-point curves are in good agreement with experimental data. The adjustable NRTL parameters were obtained by fitting the whole experimental vapor pressure data for all experimental temperatures and composition range using the least square method. The average relative deviations (ARD) for the 3 investigated systems given in Table 2 indicate that NRTL model can be used to represent {H₂O + ILs} binary systems with a good accuracy.

3.1.2. Heat capacity

The molar heat capacities of the three investigated binary systems were measured at temperatures ranging from 294.15 K to 338.15 K, under atmospheric pressure and over the whole range of composition. It can be observed from the supplementary material Tables S9-S11 and Figures S5-S7 a slight increase of C_p with increasing temperature. It is clear that the C_p values of pure ILs are greater than that of water. This is expected since C_p is dependent on the number of translational, vibrational, and rotational energy storage modes in the molecule, and the molecular weight of the ILs is much greater than water. The heat capacity of the mixtures decreases with increasing water mole fraction. This trend agrees with those reported in the literature [38–40].

Generally speaking, the heat capacities for all the binary systems studied are low, which is beneficial to heat transfer, reduce energy consumption and could improve the coefficient of performance (COP) in absorption cycles [9,41].

From heat capacity experimental data of pure IL and their mixtures with water, the excess heat capacities C_p^E can be calculated by subtracting off the ideal mixture component:

$$C_p^E = C_p - \sum_i x_i * C_{p,i} \quad (6)$$

C_p^E data were fitted to Redlich–Kister polynomials of the form:

$$C_p^E = x_2 * (1 - x_2) * \sum_i^n B_i * (x_1 - x_2)^{(i-1)} \quad (7)$$

$$\text{where } B_i = a_i + b_i * T(K) \quad (8)$$

C_p^E is the excess heat capacity $\text{J.mol}^{-1}.\text{K}^{-1}$ of the mixture; x_i is the mole fraction of species i (where $i = 1, 2$), a_i and b_i are the regressive parameter, T is the absolute temperature in K. The number of terms (B_i) in Eq. (7) depends on the degree of complexity of the binary systems. In this work, five terms in Eq. (7) were found to satisfactory correlate the C_p^E data. As represented in Figures S8-S10, Eq. (7) successfully represents the temperature and composition dependence of the excess molar heat capacity for the studied binary systems. The C_p^E for all the studied $\{\text{H}_2\text{O} + \text{IL}\}$ binary systems have both positive and negative values with maxima at low and high ILs mole fractions and a minimum at intermediate composition and a positive temperature dependence. The C_p^E values for the $\{\text{H}_2\text{O} + [\text{EMIM}][\text{EPh}]\}$ binary system have also positive and negative values with maxima at low (≈ 0.1) and intermediate IL mole fractions and a minimum at high IL concentration.

3.1.3. Density (ρ) and Excess molar volume V^E

The density of the three binary mixtures are measured in the whole range of molar concentration and in the range of temperature between 293.15 and 323.15K at atmospheric pressure. A thorough collection of respective data is presented in the Supplementary material Figure S11 and Tables S12-S14. All data were regressed using Eq. (9) [34].

$$\rho = \sum_{i=0}^3 (a_i + b_i T) x_2^i \quad (9)$$

Where ρ is the density of the solution in g.cm^{-3} , T is the absolute temperature in K, a_i and b_i are the regression parameters, and x_2^i is the molar fraction of the ILs. The regression parameters adjusted by a least-square method are listed in Table 4. The ARD between the experimental and calculated values range between 0.06 and 0.23 % (Figure S8). The density values decrease with increasing temperature and decreasing ILs molar fraction. As a whole, the density of the studied ILs roughly ranges within 1.06 and 1.33 g.cm^{-3} . Increasing the length of the alkyl chain decreases the density of the IL. Indeed, it was found that the density of the investigated binary systems decreases according to the following trend: [DMIM][MPh] > [EMIM][MPh] > [EMIM][EPh]. The experimental density data were used to calculate the excess molar volume V^E by using Eq. (10).

$$V^E = V_m - \sum_i x_i V_i^* \quad (10)$$

Where V_m is the molar volume of the mixture, and x_i, V_i^* represent the mole fraction and the molar volume of component i , respectively.

The evolution of excess molar volume versus the molar fraction of water of the three binary mixtures are illustrated in Figure S12. The three studied binary systems present asymmetrical curves. This behavior is quite common with mixtures containing two components with a large molar volume difference [42,43]. The studied binary systems showed a wavy V^E shape with a minimum level at moderate (≈ 0.4) mole fraction of ILs. Negative V^E values are obtained for the three studied binary systems. Negative V^E values were also found in literature for the binary systems containing imidazolium-based ionic liquid [44–47]. The change from negative to positive in the V^E behavior was observed

with two binary systems [DMIM][MPh] and [EMIM][EPh]. These results agree well with the behavior observed in the literature [46,47]. Experimental measurements show that an increase of the alkyl chain length of the cation leads to small V^E :

$$V^E(\text{cm}^3 \cdot \text{mol}^{-1}) = x_1 x_2 \sum_{i=1}^3 B_i (x_1 - x_2)^{i-1} \quad (11)$$

$$B_i = a_i + b_i(T(K)) \quad (12)$$

Regression parameters of Eqs. (11-12) are listed in Table 5. It is found that the calculated values are significantly consistent with the experimental data (Figure S12).

3.1.4. Excess molar Enthalpy (H^E)

Excess molar enthalpies, H^E of three binary systems are given in Table S15 and illustrated in the supporting materials (Figures S13-S14). Negative enthalpies found for all systems at $T = 312.92$ K suggest that the water/IL interactions are stronger than the corresponding IL/IL and water/water interactions. It is now well established that the effect of cation on physical properties is less significant than the anion. It is interesting to note that both [DMIM]⁺ based ILs show a slightly lower negative excess enthalpy than [EMIM]⁺ based ILs. These results are due to the longer alkyl chain length in [EMIM]⁺ than in [DMIM] leading to a stronger hydrophobic effect than the hydration effect. The repulsive interactions between the water molecules and the cation lead to exothermic systems [37-38]. For [EMIM]⁺ based ILs, the exothermic behavior of {H₂O + IL} increases in the following order: [EPh] < [MPh]. The excess enthalpies decrease with the increasing hydrophilicity of the anions or the hydrogen bonding acceptor ability. This behavior agrees well with molecular simulations [36]. All H^E experimental data are correlated using the Redlich-Kister equation:

$$H^E/x_1 x_2 = \sum_{i=1}^4 A_i * (2x_1 - 1)^{i-1} \quad (13)$$

Regression parameters are listed in Table 6.

4. Performance simulation of the absorption heat transformer cycle

The single stage AHT with solution heat exchanger studied in this work was fully described in our previous works [6,9] in which assumptions, operating conditions and thermodynamic relations are given. A schematic representation of the AHT is given in Figure 1 and indicates the index associated with each stream. In the simulation, the temperature of the evaporator T_E , condenser T_C , absorber T_A and generator T_G are set to 353K, 293K, 403K, and 353K, respectively. The characteristics of the fluids for each points of the cycle are determined through mass and energy balance equations and phase equilibrium considerations.

For sake of simplicity, the mass flowrate of vapor produced in the generator, \dot{m}_1 , is arbitrarily fixed to 1 kg/s. Hence, we have the following relationship:

$$\dot{m}_1 = \dot{m}_2 = \dot{m}_3 = \dot{m}_4 = 1 \text{ kg/s} \quad (14)$$

It is first necessary to determine the working pressures. Since pure water vapor is condensing in the condenser which temperature is T_C , it comes:

$$p_C = p_w^s(T_C) \quad (15)$$

with $p_w^s(T)$ the saturated pressure of pure water.

Similarly, in the evaporator, pure liquid water is vaporizing at temperature T_E which leads to the following relation:

$$p_E = p_w^s(T_E) \quad (16)$$

With these pressures determined, it is easy to obtain the pressures on each point of the cycle:

$$p_1 = p_2 = p_7 = p_8 = p_C \quad (17)$$

$$p_3 = p_4 = p_5 = p_6 = p_9 = p_{10} = p_E \quad (18)$$

Since the temperatures in the apparatus are fixed, it is possible to obtain the temperature of their output streams:

$$T_2 = T_C \quad (19)$$

$$T_4 = T_E \quad (20)$$

$$T_5 = T_A \quad (21)$$

$$T_8 = T_G \quad (22)$$

At the liquid outlet of the generator (stream 8) a saturated liquid solution (strong solution) is obtained. It is then possible to obtain its composition x_8^m by solving the following equation:

$$p_8 = p_{sol}^s(T_8, x_8^m) \quad (23)$$

Similarly, the weak solution outgoing the absorber is also a saturated liquid solution. Its composition, x_5^m , is obtained by solving:

$$p_5 = p_{sol}^s(T_5, x_5^m) \quad (24)$$

In the throttle valve, the pump and the solution heat exchanger the solution composition remains unchanged:

$$x_5^m = x_6^m = x_7^m \quad (25)$$

$$x_8^m = x_9^m = x_{10}^m \quad (26)$$

Solution and IL mass balances in the generator (equations 27 and 28 respectively) allow to obtain strong and weak solution mass flowrates (\dot{m}_7 and \dot{m}_8 respectively) and the weak solution composition (x_7^m):

$$\dot{m}_7 - \dot{m}_1 - \dot{m}_8 = 0 \quad (27)$$

$$\dot{m}_7 \cdot x_7^m = \dot{m}_8 \cdot x_8^m \quad (28)$$

In the throttle valve, the pump and the solution heat exchanger the solution mass flowrate remains unchanged:

$$\dot{m}_5 = \dot{m}_6 = \dot{m}_7 \quad (29)$$

$$\dot{m}_8 = \dot{m}_9 = \dot{m}_{10} \quad (30)$$

The minimum temperature difference between the weak and strong solutions in the solution heat exchanger is fixed at 5°C. Since the weak solution (hot fluid) has a higher flowrate than the strong solution (cold fluid), the minimum temperature difference is on the hot fluid side. The following relation can be obtained:

$$T_5 - T_{10} = 5^\circ\text{C} \quad (31)$$

The pumping process can be considered isothermal:

$$T_2 = T_3 \quad (32)$$

$$T_8 = T_9 \quad (33)$$

The enthalpy of the weak solution outgoing the heat exchanger (h_6) is calculated with the heat balance equation on this apparatus (equation 34). From the enthalpy value, the temperature T_6 can be deduced.

$$\dot{m}_5 \cdot h_5 + \dot{m}_9 \cdot h_9 - \dot{m}_6 \cdot h_6 - \dot{m}_{10} \cdot h_{10} = 0 \quad (34)$$

During the throttling process the enthalpy remains constant:

$$h_6 = h_7 \quad (35)$$

The knowledge of h_7 allows us to determine the temperature and the precise physical state of the weak solution at the inlet of the generator.

The heat flows exchanged with heat wells and sources can be obtained by establishing the heat balance equation in the generator, the condenser, the evaporator and the absorber respectively:

$$Q_G + \dot{m}_7 \cdot h_7 - \dot{m}_8 \cdot h_8 - \dot{m}_1 \cdot h_1 = 0 \quad (36)$$

$$\dot{m}_1 \cdot h_1 - \dot{m}_2 \cdot h_2 - Q_C = 0 \quad (37)$$

$$\dot{m}_4 \cdot h_4 - \dot{m}_3 \cdot h_3 - Q_E = 0 \quad (38)$$

$$\dot{m}_4 \cdot h_4 + \dot{m}_{10} \cdot h_{10} - \dot{m}_5 \cdot h_5 - Q_A = 0 \quad (39)$$

The performance of single stage absorption heat transformers (SSAHT) operating with the new aforementioned working fluid pairs at given operating conditions could be assessed by different parameters such as coefficient of performance COP, circulation ratio (f) and gross temperature lift ΔT .

Coefficient of performance (COP) is the essential parameter and it could be defined as the ratio of the heat output (upgraded high temperature heat) at the absorber, per the input heat (medium temperature heat) at the generator and evaporator.

$$COP = \frac{Q_A}{Q_G + Q_E} \quad (40)$$

Another fundamental parameter is the gross temperatures lift Δt which is the difference between the temperature level of the produced upgraded heat (T_A) and the waste heat temperature ($T_E = T_G$). ΔT provides qualitative description of the cycle upgrading potential.

$$\Delta t = T_A - T_E \quad (41)$$

Circulation ratio (f) is an important parameter while it evaluates the cycle components cost, energy and heating, pumping processes and operating expenses. It is defined as the ratio of mass flow rate of the strong solution produced by the generator, per unit mass of refrigerant vapor produced by the generator.

$$f = \dot{m}_8 / \dot{m}_1 \quad (42)$$

Additionally, the available heat output (q) per unit mass of refrigerant could be presented as:

$$q = Q_A / \dot{m}_1 \quad (43)$$

The simulation results for the new working binary systems are shown in Table 7.

In this section, the simulation results for AHT using the three new alternative working fluids are compared to each other and to the data found in literature for the conventional working fluid {H₂O + LiBr}.

In this study, evaporator temperature T_E , condenser temperature T_C , absorber temperature T_A and generator temperature T_G were set to 80 °C, 20 °C, 130 °C, and 80 °C, respectively. On the other hand, the components temperatures (T_G , T_E , T_A , T_C) values were modified in order to investigate the influence of each on the performance of the AHT.

Simulation results for evaporator temperature T_E , condenser temperature T_C , absorber temperature T_A and generator temperature T_G set to 80°C, 25°C, 130°C, and 80°C respectively, showed that the COP values for the studied binary systems have the following trend comparing to {H₂O + LiBr}:

$$\{\text{H}_2\text{O} + \text{LiBr}\} > \{\text{H}_2\text{O} + [\text{DMIM}][\text{MeSO}_4]\} > \{\text{H}_2\text{O} + [\text{EMIM}][\text{MPh}]\} > \{\text{H}_2\text{O} + [\text{DMIM}][\text{MPh}]\} > \{\text{H}_2\text{O} + [\text{EMIM}][\text{EPh}]\}.$$

It seems that the anion has a stronger influence on the performances and that small alkyl chain length on the anion gives better results. The behavior was already observed in previous work. [6]

The simulation results at different operating temperatures show that the COP of the investigated binary systems are between 5 and 12% lower than that for the conventional working {H₂O + LiBr} pairs. If this is not in favor of the choice of IL as an absorbent, it must be kept in mind several other facts. First, the difference in COP with {H₂O+LiBr} is relatively small. Moreover, the research of alternative working pairs aims at overcoming the corrosiveness of LiBr and the risk of crystallization of LiBr at certain temperatures and solution compositions. The working pairs proposed in this study are miscible in all proportions and the risk of crystallization is totally avoided. Dialkylimidazolium alkylphosphonate ILs are known to be compatible with the most common construction metals such as carbon and stainless steel. [30] Finally, the temperature range of use of the proposed working mixtures is extended compared to {H₂O+LiBr}. Due to its high corrosivity, it is difficult to use LiBr solution at high temperatures which is not the case with the proposed mixtures.

Temperatures of the cycle components have a significant impact on the COP. At given absorber and generator temperatures. Figure 2 shows that COP is almost constant as the condenser temperature rises up to about 303.15 K, followed by a sharp drop as T_c increases above 303.15 K. This behavior occurs due to the relation between the condenser temperature and the concentration of the refrigerant in the strong solution which could be clarified by the following VLE equation in the generator:

$$x_8 = \frac{p_c}{\gamma_w p^s(T_8)} \quad (44)$$

Where x_8 is the mole fraction of ILs at point 8 (strong solution), p_c is the vapor pressure at the condenser, γ_w is the activity coefficient of the refrigerant and $p^s(T_8)$ is the saturated vapor pressure at T_8 . As T_c increases, accordingly, the system low pressure will increase and the ILs mole fraction in the strong solution will decrease. Therefore, the strong solution concentration will decrease and circulation ratio will increase and COP will drop sharply. The classically used {H₂O + LiBr} has the same behavior as the proposed mixtures, but the sharp decrease of COP is even more abrupt and happens for a lower condenser temperature. Using ILs as absorbents allows to work with higher condenser temperature and maintaining an almost constant value of the COP. This could

be an asset when the temperature of the cold heat well varies significantly during the operation of the AHT (for seasonal reasons for instance). Between the three studied mixtures, {H₂O+[EMIM][MPh]} is the one which allow to extend the most the usable condenser temperature range. Nevertheless, the two alkylsulphate based ILs proposed for comparison give better results than their phosphonate counterparts.

A similar behavior could be noticed when varying the absorber temperature (with the other temperatures remaining constant). As can be seen on Figure 3, when T_A increases up to about 400 K, COP decreases very slowly (Figure 3) and after 400 K decreases sharply. This means that for those values of T_C and T_G=T_E, the waste heat can efficiently be upgraded to 400K with corresponds to a temperature lift of about 50 K. Higher temperature lift can be obtained but with a poor efficiency. The absorber temperature (T_A = T_H) has direct influence on the concentration of the weak solution. The strong solution which is produced in the generator and pumped towards the absorber has a high absorbent (IL) concentration which facilitates absorption process of the refrigerant vapor at the absorber. At constant condenser and generator temperatures, mass fraction of ILs in the weak solution x_w^m increases with T_A. Accordingly, concentration difference $\Delta x^m = x_8^m - x_5^m$ decreases, circulation ratio (f) and pumping power increases.

The comparison with {H₂O+LiBr} is noteworthy since it allows to identify that {H₂O+[EMIM][MPh]} allows to reach higher absorber temperature, and consequently temperature lift, while maintaining significant values of COP. It is also noticeable that the {H₂O+[DMIM][MeSO₄]} and {H₂O+[EMIM][MeSO₄]} give better results than the phosphonated ILs based mixtures.

As can be expected, the evaporator (or generator) temperature (T_E = T_G) has a different influence on the AHT COP. At constant absorber and condenser temperatures, COP increases sharply as the T_E increases, then gradually it becomes stable and finally it slightly reduces as shown in Figure 4. The evaporator temperature (T_E) has direct impact on the high pressure levels of the AHT cycle and the weak solution concentration. Increasing T_E or T_G leads to a decline of the weak solution concentration, hence, circulation ratio decreases and COP becomes higher. It is also interesting to notice that

using ILs based mixtures allow to upgraded colder medium temperature (evaporator temperature) heat than what is possible with {H₂O+LiBr}. This is an advantage to ensure a steady operation with a waste heat source that has an unsteady temperature. Once again, {H₂O +[EMIM][MPh]} presents the best performances of the three studied mixtures and is comparable to the alkylsulphate ILs based mixtures.

For the comparison with other AHT working mixture to be complete, it is necessary to discuss the values of f , the circulation ratio. Due to their high molecular weight, it can be seen on Table 7, that values for ILs based mixture is generally significantly higher than for the reference mixture {H₂O+LiBr}. This can be problematic because a higher value of f combined with the high viscosity of IL concentrated solution lead to significantly increased pumping costs and consequently a reduced value of COP. As previously mentioned, dialkylimidazolium alkylphosphonate have relatively low viscosities compared to other ILs. Moreover, {H₂O +[EMIM][MPh]} which is the best candidate amongst the three studied mixtures allow to operate with moderate values of f . The evaluation of the pumping costs is a delicate problem since it requires to know the layout of the piping in the real AHT and a precise cost evaluation study must be achieved to be meaningful and is over the frame of the theoretical study of the AHT cycle.

Finally, results presented in Table 7 enables to see that the proposed IL based mixtures give better performances are better than other alternative mixtures such as {NH₃+H₂O} and {TFE + E181}.

Conclusion

Three binary systems consisting of {H₂O + alkylphosphonate based IL} basic thermodynamic properties including vapor pressure, heat capacity, excess enthalpy, density were measured. The VLE values of these 3 binary solutions showed a considerable negative deviation from Raoult's law, which is an important characteristic for absorption heat transformers working fluids. The excess enthalpies data measured of the binary systems at different IL concentrations and at different temperatures were negative. NRTL model and correlations used in this work for the representation of thermodynamic properties allow to represent experimental data with good accuracy.

Simulation of a single stage AHT shows that the performance in term of COP of {H₂O + alkylphosphonate based IL} working fluids is lower (about 10%) than {H₂O + LiBr}. Nevertheless, {H₂O+[EMIM][MPH]} both allows to reach higher temperature lift and to use a lower temperature waste heat source which guarantee a better operation stability. The high circulation ratio and the significantly higher viscosity of ILs compared to conventional working pairs is nevertheless a drawback of the proposed mixture. This problem requires a precise cost evaluation to assess the use of IL in AHT. Finally, corrosion caused by LiBr solutions could be avoided using alkylphosphonate based ILs.

5. References

- [1] K. Parham, M. Khamooshi, D.B.K. Tematio, M. Yari, U. Atikol, Absorption heat transformers - A comprehensive review, *Renewable and Sustainable Energy Reviews*. 34 (2014) 430–452. <https://doi.org/10.1016/j.rser.2014.03.036>.
- [2] H. Noubli, D. Alonso, V. Renaudin, T. Cachot, Development of a new absorption-demixing heat transformer: Cycle and working mixture optimization, *International Journal of Chemical Reactor Engineering*. 8 (2010).
- [3] D. Alonso, T. Cachot, J.-M. Hornut, Performance simulation of an absorption heat transformer operating with partially miscible mixtures, *Applied Energy*. 72 (2002) 583–597. [https://doi.org/10.1016/S0306-2619\(02\)00052-1](https://doi.org/10.1016/S0306-2619(02)00052-1).
- [4] A. Acevedo, J.A. Hernandez, D. Juarez, A. Parrales, R. Saravanan, A. Huicochea, Thermodynamic analysis of cooling and heating systems for energy recovery, *International Journal of Refrigeration*. 115 (2020) 172–181. <https://doi.org/10.1016/j.ijrefrig.2020.02.034>.
- [5] Z. Xu, R. Wang, Absorption heat pump for waste heat reuse: current states and future development, *Front. Energy*. 11 (2017) 414–436. <https://doi.org/10.1007/s11708-017-0507-1>.
- [6] E.-S. Abumandour, F. Mutelet, D. Alonso, Are Ionic Liquids Suitable as New Components in Working Mixtures for Absorption Heat Transformers?, *Progress and Developments in Ionic Liquids*. (2017). <https://doi.org/10.5772/65756>.
- [7] J. Sun, L. Fu, S. Zhang, A review of working fluids of absorption cycles, *Renewable and Sustainable Energy Reviews*. 16 (2012) 1899–1906. <https://doi.org/10.1016/j.rser.2012.01.011>.
- [8] N.V. Plechkova, K.R. Seddon, Applications of ionic liquids in the chemical industry, *Chem. Soc. Rev*. 37 (2007) 123–150. <https://doi.org/10.1039/B006677J>.
- [9] E.-S. Abumandour, F. Mutelet, D. Alonso, Performance of an absorption heat transformer using new working binary systems composed of {ionic liquid and water}, *Applied Thermal Engineering*. 94 (2016) 579–589. <https://doi.org/10.1016/j.applthermaleng.2015.10.107>.
- [10] D. Zheng, L. Dong, W. Huang, X. Wu, N. Nie, A review of imidazolium ionic liquids research and development towards working pair of absorption cycle, *Renewable and Sustainable Energy Reviews*. 37 (2014) 47–68. <https://doi.org/10.1016/j.rser.2014.04.046>.
- [11] Z. He, Z. Zhao, X. Zhang, H. Feng, Thermodynamic properties of new heat pump working pairs: 1,3-Dimethylimidazolium dimethylphosphate and water, ethanol and

- methanol, *Fluid Phase Equilibria*. 298 (2010) 83–91. <https://doi.org/10.1016/j.fluid.2010.07.005>.
- [12] E. Vataščin, V. Dohnal, Phase equilibria and energetics of binary mixtures of water with highly hydrophilic [EMIM]-based ionic liquids: Methanesulfonate, methylsulfate, and dimethylphosphate, *Fluid Phase Equilibria*. 521 (2020). <https://doi.org/10.1016/j.fluid.2020.112659>.
- [13] E. Vataščin, V. Dohnal, Phase equilibria of (water + [EMIM] bromide) and (water + [EMIM] tosylate), *Fluid Phase Equilibria*. 483 (2019) 84–91. <https://doi.org/10.1016/j.fluid.2018.11.001>.
- [14] E. Vataščin, V. Dohnal, Thermodynamic properties of aqueous solutions of [EMIM] thiocyanate and [EMIM] dicyanamide, *Journal of Chemical Thermodynamics*. 106 (2017) 262–275. <https://doi.org/10.1016/j.jct.2016.12.008>.
- [15] E. Vataščin, V. Dohnal, Thermophysical properties of aqueous solutions of the 1-ethyl-3-methylimidazolium tricyanomethanide ionic liquid, *Journal of Chemical Thermodynamics*. 89 (2015) 169–176. <https://doi.org/10.1016/j.jct.2015.05.011>.
- [16] E. Vataščin, V. Dohnal, Aqueous solutions of [EMIM] 1,1,2,2-tetrafluoroethanesulfonate and [EMIM] trifluoromethanesulfonate: A thermodynamic study, *Journal of Chemical Thermodynamics*. 119 (2018) 114–126. <https://doi.org/10.1016/j.jct.2017.12.019>.
- [17] M. Wang, C.A. Infante Ferreira, Absorption heat pump cycles with NH₃ – ionic liquid working pairs, *Applied Energy*. 204 (2017) 819–830. <https://doi.org/10.1016/j.apenergy.2017.07.074>.
- [18] Y. Sun, G. Di, J. Wang, Y. Hu, X. Wang, M. He, Gaseous solubility and thermodynamic performance of absorption system using R1234yf/IL working pairs, *Applied Thermal Engineering*. 172 (2020) 115161. <https://doi.org/10.1016/j.applthermaleng.2020.115161>.
- [19] C. Song, X. Liu, Z. Ye, M. He, A new power/cooling cogeneration system using R1234ze(E)/ionic liquid working fluid, *International Journal of Energy Research*. 44 (2020) 4703–4716. <https://doi.org/10.1002/er.5252>.
- [20] X. Liu, Z. Ye, L. Bai, M. He, Performance comparison of two absorption-compression hybrid refrigeration systems using R1234yf/ionic liquid as working pair, *Energy Conversion and Management*. 181 (2019) 319–330. <https://doi.org/10.1016/j.enconman.2018.12.030>.
- [21] W. Chen, S. Liang, Thermodynamic analysis of absorption heat transformers using [mmim]DMP/H₂O and [mmim]DMP/CH₃OH as working fluids, *Applied Thermal Engineering*. 99 (2016) 846–856. <https://doi.org/10.1016/j.applthermaleng.2016.01.135>.
- [22] S.M.S. Murshed, C.A.N. de Castro, M.J.V. Lourenço, J. França, A.P.C. Ribeiro, S.I.C. Vieira, C.S. Queirós, Ionanofluids as novel fluids for advanced heat transfer applications, *World Academy of Science, Engineering and Technology*. 76 (2011) 795–798.
- [23] A.A. Minea, S.M.S. Murshed, A review on development of ionic liquid based nanofluids and their heat transfer behavior, *Renewable and Sustainable Energy Reviews*. 91 (2018) 584–599. <https://doi.org/10.1016/j.rser.2018.04.021>.
- [24] J.M.P. Franca, M.J.V. Lourenco, M. Sohel Murshed, A.A.H. Padua, C.A. Nieto de Castro, Thermal conductivity of ionic liquids and ionanofluids and their feasibility

- as heat transfer fluids, *Industrial and Engineering Chemistry Research*. 57 (2018) 6516–6529. <https://doi.org/10.1021/acs.iecr.7b04770>.
- [25] C. Luo, Y. Wang, Y. Li, Y. Wu, Q. Su, T. Hu, Thermodynamic properties and application of LiNO₃-[MMIM][DMP]/H₂O ternary working pair, *Renewable Energy*. 134 (2019) 147–160. <https://doi.org/10.1016/j.renene.2018.10.104>.
- [26] D. Yang, Y. Zhu, S. Liu, H. Lv, C. Luo, Thermodynamic Properties of a Ternary AHP Working Pair: Lithium Bromide + 1-Ethyl-3-methylimidazolium Chloride + H₂O, *Journal of Chemical and Engineering Data*. 64 (2019) 574–583. <https://doi.org/10.1021/acs.jced.8b00771>.
- [27] E.-S.R.E. Hassan, F. Mutelet, J.-C. Moïse, N. Brosse, Pretreatment of miscanthus using 1,3-dimethyl-imidazolium methyl phosphonate (DMIMMPH) ionic liquid for glucose recovery and ethanol production, *RSC Adv*. 5 (2015) 61455–61464. <https://doi.org/10.1039/C5RA08946H>.
- [28] K. Kêdra-Królik, M. Fabrice, J.-N. Jaubert, Extraction of thiophene or pyridine from n-heptane using ionic liquids. gasoline and diesel desulfurization, *Industrial and Engineering Chemistry Research*. 50 (2011) 2296–2306. <https://doi.org/10.1021/ie101834m>.
- [29] J.M. Lopes, M.D. Bermejo, Á. Martín, M.J. Cocero, Ionic Liquid as Reaction Media for the Production of Cellulose-Derived Polymers from Cellulosic Biomass, *ChemEngineering*. 1 (2017) 10. <https://doi.org/10.3390/chemengineering1020010>.
- [30] I. Murrieta-Pazos, E. Husson, L. Dupont, G. Marlair, M. Nonus, C. Len, N. Thiebault, J. Garcia, B. Narcy, C. Sarazin, I. Gosselin, Corrosive properties of liquid fractions issued from lignocellulosic biomass pretreatment with ionic liquids, in: 2016. <https://hal-ineris.archives-ouvertes.fr/ineris-01854728> (accessed July 16, 2020).
- [31] P. Kneisl, J.W. Zondlo, Vapor Pressure, Liquid Density, and the Latent Heat of Vaporization as Functions of Temperature for Four Dipolar Aprotic Solvents, *Journal of Chemical and Engineering Data*. 32 (1987) 11–13. <https://doi.org/10.1021/je00047a003>.
- [32] M.-A. Michou-Saucet, J. Jose, C. Michou-Saucet, J.C. Merlin, Pressions de vapeur et enthalpies libres d'excès de systemes binaires: Hexamethylphosphorotriamide (HMPT) + n-hexane; n-heptane; n-octane: A 298,15 K; 303,15 K; 313,15 K; 323,15 K; 333,15 K, *Thermochimica Acta*. 75 (1984) 85–106. [https://doi.org/10.1016/0040-6031\(84\)85009-1](https://doi.org/10.1016/0040-6031(84)85009-1).
- [33] J.L. Oscarson, S.O. Lundell, J.R. Cunningham, PHASE EQUILIBRIA FOR TEN BINARY SYSTEMS., *AIChE Symposium Series*. 83 (1987) 1–17.
- [34] N. Nie, D. Zheng, L. Dong, Y. Li, Thermodynamic properties of the water + 1-(2-hydroxyethyl)-3- methylimidazolium chloride system, *Journal of Chemical and Engineering Data*. 57 (2012) 3598–3603. <https://doi.org/10.1021/je3007953>.
- [35] H. Passos, I. Khan, F. Mutelet, M.B. Oliveira, P.J. Carvalho, L.M.N.B.F. Santos, C. Held, G. Sadowski, M.G. Freire, J.A.P. Coutinho, Vapor-liquid equilibria of water + alkylimidazolium-based ionic liquids: Measurements and perturbed-chain statistical associating fluid theory modeling, *Industrial and Engineering Chemistry Research*. 53 (2014) 3737–3748. <https://doi.org/10.1021/ie4041093>.
- [36] L.E. Ficke, J.F. Brennecke, Interactions of ionic liquids and water, *Journal of Physical Chemistry B*. 114 (2010) 10496–10501. <https://doi.org/10.1021/jp1012736>.

- [37] H. Renon, J.M. Prausnitz, Local compositions in thermodynamic excess functions for liquid mixtures, *AIChE Journal*. 14 (1968) 135–144. <https://doi.org/10.1002/aic.690140124>.
- [38] H.-C. Hu, A.N. Soriano, R.B. Leron, M.-H. Li, Molar heat capacity of four aqueous ionic liquid mixtures, *Thermochimica Acta*. 519 (2011) 44–49. <https://doi.org/10.1016/j.tca.2011.02.027>.
- [39] G. García-Miaja, J. Troncoso, L. Romání, Excess enthalpy, density, and heat capacity for binary systems of alkylimidazolium-based ionic liquids + water, *Journal of Chemical Thermodynamics*. 41 (2009) 161–166. <https://doi.org/10.1016/j.jct.2008.10.002>.
- [40] L.E. Ficke, H. Rodríguez, J.F. Brennecke, Heat capacities and excess enthalpies of 1-ethyl-3-methylimidazolium-based ionic liquids and water, *Journal of Chemical and Engineering Data*. 53 (2008) 2112–2119. <https://doi.org/10.1021/je800248w>.
- [41] X. Zhang, D. Hu, Performance analysis of the single-stage absorption heat transformer using a new working pair composed of ionic liquid and water, *Applied Thermal Engineering*. 37 (2012) 129–135. <https://doi.org/10.1016/j.applthermaleng.2011.11.006>.
- [42] E.J. Gonzalez, N. Calvar, P. Fernandez, A. Dominguez, E.A. Macedo, Physical and excess properties for binary systems containing an alcohol and ionic liquid at T = 298.15 K, in: 2012.
- [43] I. Bahadur, T.M. Letcher, S. Singh, G.G. Redhi, P. Venkatesu, D. Ramjugernath, Excess molar volumes of binary mixtures (an ionic liquid + water): A review, *Journal of Chemical Thermodynamics*. 82 (2015) 34–46. <https://doi.org/10.1016/j.jct.2014.10.003>.
- [44] A. Bhattacharjee, C. Varanda, M.G. Freire, S. Matted, L.M.N.B.F. Santos, I.M. Marrucho, J.A.P. Coutinho, Density and viscosity data for binary mixtures of 1-alkyl-3-methylimidazolium alkylsulfates + water, *Journal of Chemical and Engineering Data*. 57 (2012) 3473–3482. <https://doi.org/10.1021/je300622r>.
- [45] H. Rodríguez, J.F. Brennecke, Temperature and composition dependence of the density and viscosity of binary mixtures of water + ionic liquid, *Journal of Chemical and Engineering Data*. 51 (2006) 2145–2155. <https://doi.org/10.1021/je0602824>.
- [46] E. Vercher, A.V. Orchillés, P.J. Miguel, A. Martínez-Andreu, Volumetric and ultrasonic studies of 1-ethyl-3-methylimidazolium trifluoromethanesulfonate ionic liquid with methanol, ethanol, 1-propanol, and water at several temperatures, *Journal of Chemical and Engineering Data*. 52 (2007) 1468–1482. <https://doi.org/10.1021/je7001804>.
- [47] G. Rai, A. Kumar, A reversal from endothermic to exothermic behavior of imidazolium-based ionic liquids in molecular solvents, *Chemical Physics Letters*. 496 (2010) 143–147. <https://doi.org/10.1016/j.cplett.2010.07.056>.
- [48] I. Sujatha, G. Venkatarathnam, Performance of a vapour absorption heat transformer operating with ionic liquids and ammonia, *Energy*. 141 (2017) 924–936. <https://doi.org/10.1016/j.energy.2017.10.002>.

Figure caption

Figure 1: Schematic diagram of experimental apparatus for the measurement of isobaric vapor pressure. 1. Temperature transmitter; 2. Pressure transducer (Druck-PMP4010); 3. Condenser; 4. Refrigerator; 5. Temperature sensor (T900 series); 6. Equilibrium vessel; 7. Constant temperature bath; 8. Magnetic stirrer; 9. Pressure buffer; 10. Vacuum control valve; 11. Vacuum pump.

Figure 2. Thermodynamic cycle in absorption heat transformer (AHT).

Figure 3. COP variation with the condenser temperature T_C (T_L) for single stage absorption heat transformer cycle at given T_E and T_A equal to 353.15 and 403.15 K, respectively for working pairs —: {H₂O + [DMIM][MPh]}, —: {H₂O + [EMIM][MPh]}, —: {H₂O + [EMIM][EPh]}, —: {H₂O + [DMIM][MeSO₄]}, —: {H₂O + [EMIM][MeSO₄]}, — {H₂O + LiBr}.

Figure 4. COP variation with the absorber temperature T_A (T_H) for single stage absorption heat transformer cycle at given T_C and T_E equal to 293.15 and 353.15 K, respectively for working pairs —: {H₂O + [DMIM][MPh]}, —: {H₂O + [EMIM][MPh]}, —: {H₂O + [EMIM][EPh]}, —: {H₂O + [DMIM][MeSO₄]}, —: {H₂O + [EMIM][MeSO₄]}, — {H₂O + LiBr}.

Figure 5. COP variation with the evaporator, generator temperature T_E , T_G (T_M) for single stage absorption heat transformer cycle at given T_C and T_A equal to 293.15 and 403.15 K, respectively for working pairs —: {H₂O + [DMIM][MPh]}, —: {H₂O

+ [EMIM][MPh]}, —: {H₂O + [EMIM][EPh]}, —: {H₂O + [DMIM][MeSO₄]}, —: {H₂O + [EMIM][MeSO₄]}, — {H₂O + LiBr}.

Figure 1:

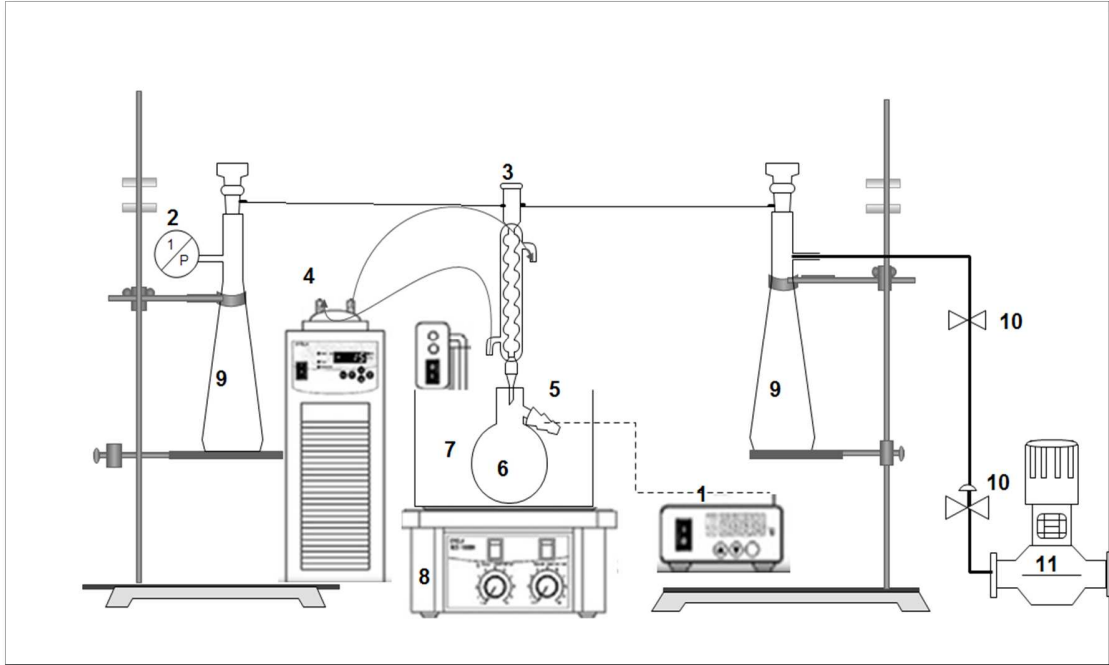


Figure 2.

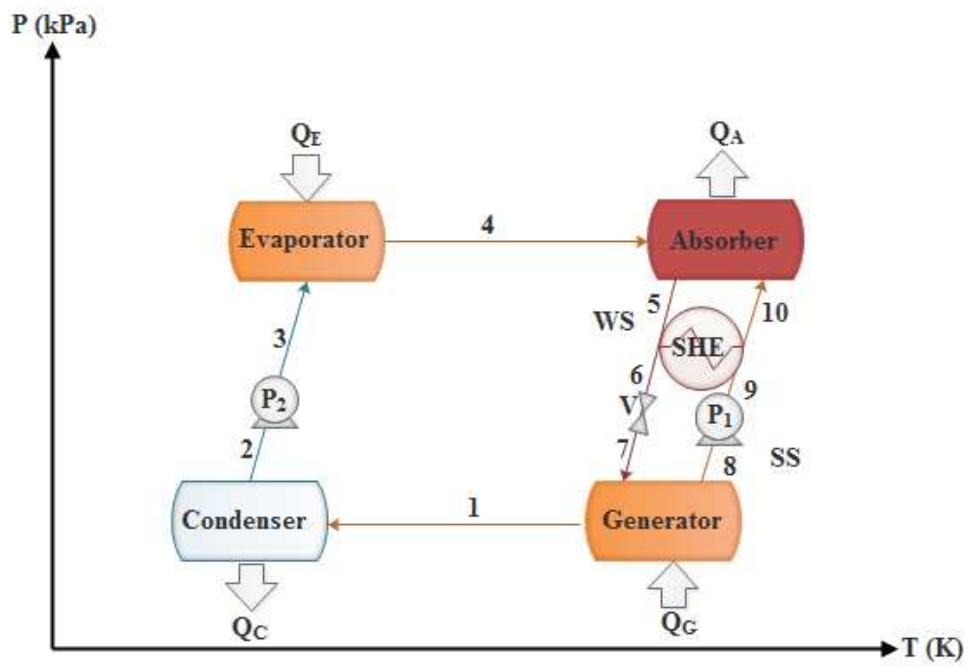


Figure 3.

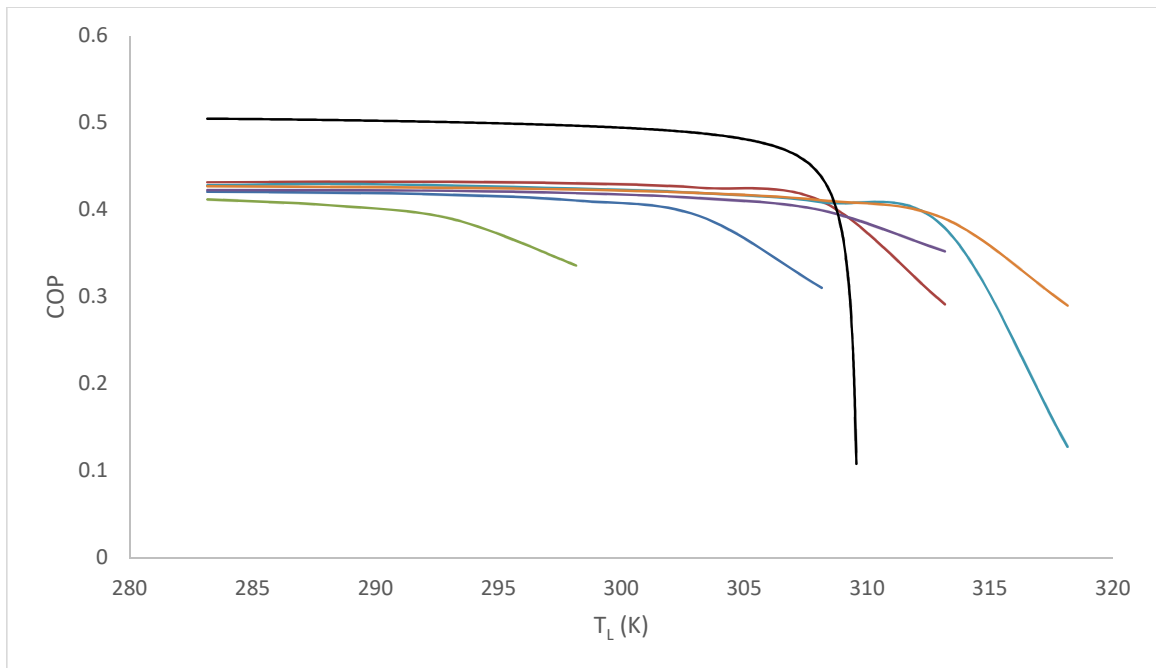


Figure 4.

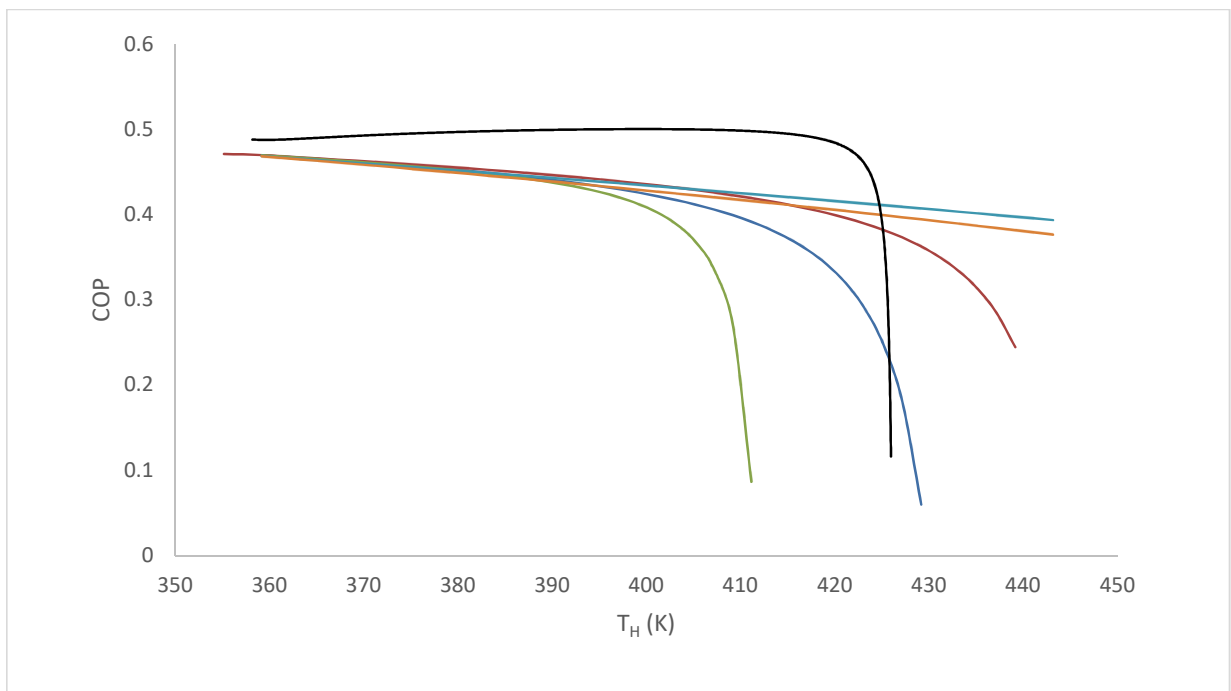


Figure 5.

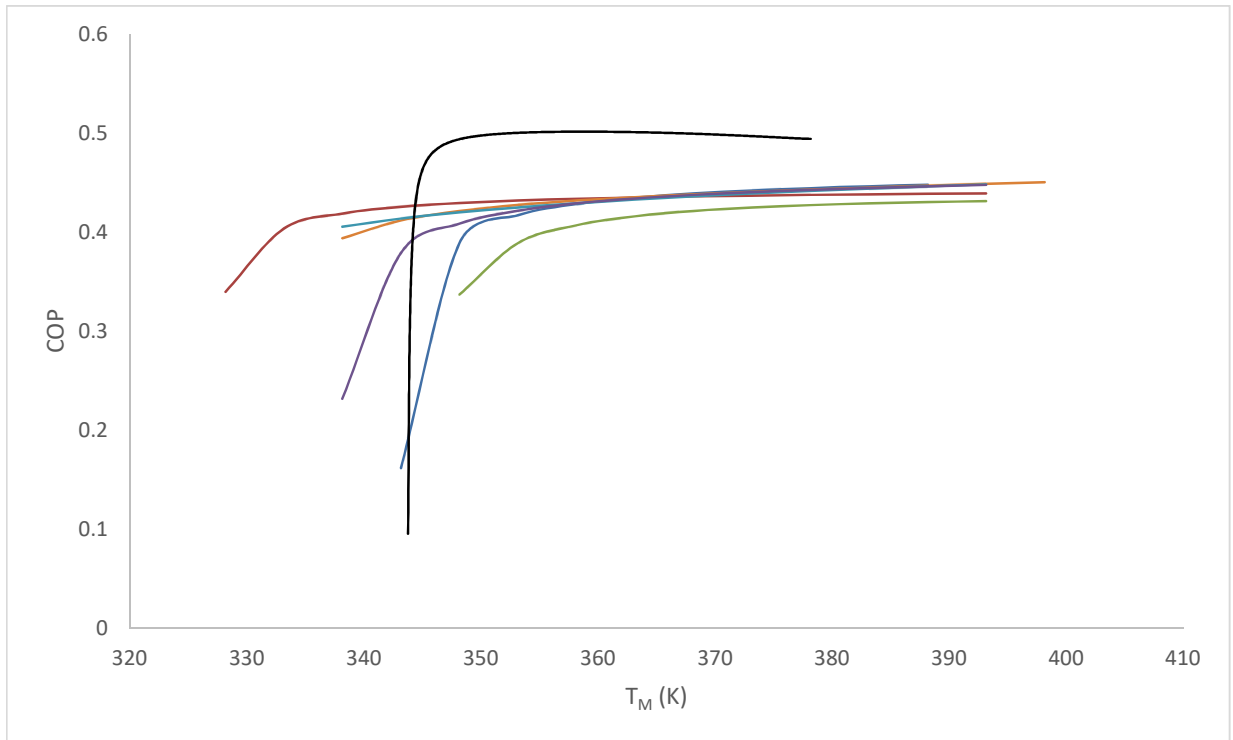


Table 1. Physical properties of the studied ionic liquids.

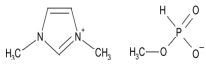
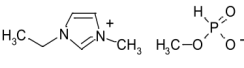
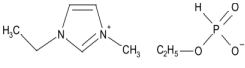
Physical Properties	[DMIM][MPh]	[EMIM][MPh]	[EMIM][EPh]
Structure			
Full name of IL	1,3-dimethylimidazolium methylphosphonate	1-ethyl-3-methylimidazolium methyl phosphonate	1-ethyl-3-methylimidazolium ethyl phosphonate
Color and shape (at 25 °C)	Yellow Liquid	Yellow Liquid	Colorless Liquid
Molecular formula	C ₆ H ₁₃ N ₂ PO ₃	C ₇ H ₁₅ N ₂ PO ₃	C ₈ H ₁₇ N ₂ PO ₃
Purity (%)	> 98	> 98	> 98
Molecular weight (g.mol ⁻¹)	192.15	206.18	220.2
Density (g.cm ⁻³)	1.18 at 20°C	n.d.	1.13 at 20°C
Viscosity (cP)	50.3 at 25°C	107 at 25°C	140 at 25°C
Decomposition temp. (°C)	> 200	n.d.	n.d.
Water content (ppm)	475.8	1161.3	704.4

Table 2. NRTL parameters of the VLE data for {H₂O + IL}.

Binary system	a ₁₂ /(J.mol ⁻¹)	a ₂₁ /(J.mol ⁻¹)	b ₁₂ /(J.mol ⁻¹)	b ₂₁ /(J.mol ⁻¹)	α	(ΔP %)
{H ₂ O + [DMIM][MPh]}	-1442.2	-4996.0	20.6	-6.8	0.3	4.5
{H ₂ O + [EMIM][MPh]}	1.0	0.9	19.3	-24.8	0.3	9.3
{H ₂ O + [EMIM][EPh]}	-27575.3	-7654.0	74.0	1.8	0.3	4.0

Table 3. Parameters for the correlation of Eq. (8).

Binary system {H ₂ O + IL}	A ₀	A ₁	A ₂	A ₃	B ₀	B ₁	B ₂	B ₃	ΔC _p %
{H ₂ O+[DMIM][MPh]}	34.22	186.54	24.49	42.97	0.06	-0.46	2.87	-2.30	2.20
{H ₂ O+[EMIM][MPh]}	31.51	178.58	182.24	-146.92	0.06	-0.30	1.53	-1.05	4.15
{H ₂ O + [EMIM][EPh]}	213.10	-1324.07	3498.91	-2187.60	-0.48	5.53	-11.91	7.41	2.68

Table 4. Parameters for the correlation of Eq. (12).

Binary system {H ₂ O + IL }	a ₀	a ₁	a ₂	a ₃	b ₀	b ₁	b ₂	b ₃	Δρ %
{H ₂ O + [DMIM][MPh]}	1.3682	0.1342	-0.0543	-0.0592	-0.0010	0.0018	-0.0031	0.0018	0.23
{H ₂ O + [EMIM][MPh]}	0.3401	0.3401	0.3401	0.3401	-0.0009	0.0014	-0.0021	0.0010	0.18
{H ₂ O + [EMIM][EPH]}	1.2843	0.0893	0.0046	-0.0586	-0.0007	0.0008	-0.0017	0.0010	0.16

Table 5. Redlich Kister parameters for the representation of V^E of binary systems {H₂O + IL}.

Binary system	a ₁	a ₂	a ₃	a ₄	a ₅	b ₁	b ₂	b ₃	b ₄	b ₅	ΔV ^E %
{H ₂ O + [DMIM][MPh]}	-3.79	-7.64	0.88	-12.72	1.20	0.00	0.01	0.02	0.03	2.10	12.12
{H ₂ O + [EMIM][MPh]}	-4.93	-13.27	5.71	-9.75	1.15	0.00	0.03	-0.02	0.04	0.20	3.58
{H ₂ O + [EMIM][EPH]}	-2.81	-12.02	-38.25	36.29	1.03	-0.01	0.03	0.13	-0.13	0.59	24.19

Table 6. Redlich-Kister parameters for H^E for {H₂O + IL}.

Binary system	A ₁	A ₂	A ₃	A ₄	ΔH ^E %
{H ₂ O + [DMIM][MPh]}	-16582.69	10105.69	-12835.62	-3168.39	2.72
{H ₂ O + [EMIM][MPh]}	-20996.20	10554.39	-5769.54	7132.76	1.28
{H ₂ O + [EMIM][EPH]}	-19034.15	10205.39	-4611.32	6153.53	1.22

Table 7: Calculated COP of {H₂O + IL} binary systems for absorption heat transformer cycle compared to data found in literature^{*,**}.

T (K)		T _C	T _E	T _G	T _A
		293.15	353.15	353.15	403.15
Refrigerant	Absorbent	COP	x ^m _s	Δx ^m	f
Water	[DMIM][MPh]	0.42	0.98	0.03	29.26
Water	[EMIM][MPh]	0.43	0.98	0.05	18.68
Water	[EMIM][EPh]	0.39	0.96	0.02	49.89
Water	[DMIM][MeSO ₄]	0.43	0.99	0.04	22.7
Water	[EMIM][MeSO ₄]	0.43	0.98	0.04	24.16
T (K)		T _C	T _E	T _G	T _A
		298.15	353.15	353.15	403.15
Refrigerant	Absorbent	COP	x ^m _s	Δx ^m	f
Water	[DMIM][MPh]	0.41	0.98	0.03	35.68
Water	[EMIM][MPh]	0.43	0.97	0.05	21.80
Water	[EMIM][EPh]	0.34	0.96	0.01	85.02
Water	[DMIM][MeSO ₄]	0.42	0.98	0.04	27.09
Water	[EMIM][MeSO ₄]	0.42	0.98	0.04	27.42
Water	LiBr*	0.48	n.d	n.d	9.51
T (K)		T _C	T _E	T _G	T _A
		308.15	363.15	363.15	403.15
Refrigerant	Absorbent	COP	x ^m _s	Δx ^m	f
Water	[DMIM][MPh]	0.44	0.97	0.05	19.73
Water	[EMIM][MPh]	0.44	0.96	0.07	13.55
Water	[EMIM][EPh]	0.43	0.96	0.04	27.04
Water	[DMIM][MeSO ₄]	0.44	0.97	0.05	21.81
Water	[EMIM][MeSO ₄]	0.43	0.97	0.04	22.76
Water	LiBr**	0.50	0.64	0.07	11.00
TFE	E181**	0.42	0.90	0.10	9.00
T (K)		TC	TE	TG	TA
		298.15	343.15	343.15	373.15
Refrigerant	Absorbent	COP	x ^m _s	Δx ^m	f
Water	[DMIM][MPh]	0.45	0.96	0.06	19.73
Water	[EMIM][MPh]	0.46	0.95	0.08	11.77
Water	[EMIM][EPh]	0.45	0.94	0.02	2042.29
Water	LiBr***	0.50	n.d.	n.d.	5.10
NH ₃	Water	0.40	n.d.	n.d.	3.24

*Data found in literature [1]

**Data found in literature [41]

***Data found in literature [48]